Off-site control of repolarization alternans in cardiac fibers

Trine Krogh-Madsen,[1,*] Alain Karma,[2] Mark L. Riccio,[3] Peter N. Jordan,[4] David J. Christini,[1,4] and Robert F. Gilmour, Jr.[3]

[1]*Greenberg Division of Cardiology, Department of Medicine, Weill Cornell Medical College, New York, New York 10021, USA*
[2]*Department of Physics and Center for Interdisciplinary Research on Complex Systems,*
Northeastern University, Boston, Massachusetts 02115, USA
[3]*Department of Biomedical Sciences, College of Veterinary Medicine, Cornell University, Ithaca, New York 14853, USA*
[4]*Department of Physiology and Biophysics, Weill Cornell Medical College, New York, New York 10021, USA*

Repolarization alternans, a beat-to-beat alternation in action potential duration, has been putatively linked to the onset of cardiac reentry. Anti-alternans control strategies can eliminate alternans in individual cells by exploiting the rate dependence of action potential duration. The same approach, when applied to a common measuring/stimulating site at one end of a cardiac fiber, has been shown to have limited spatial efficacy. As a first step toward spatially distributed electrode control systems, we investigated "off-site" control in canine Purkinje fibers, in which the recording and control sites are different. We found experimentally that alternans can be eliminated at, or very near, the recording site, and that varying the location of the recording site along the fiber causes the node (the location with no alternans) to move along the fiber in close proximity to the recording site. Theoretical predictions based on an amplitude equation [B. Echebarria and A. Karma, Chaos **12**, 923 (2002)] show that those findings follow directly from the wave nature of alternans: the most unstable mode of alternans along the fiber is a wave solution of a one-dimensional Helmholtz equation with a node position that only deviates slightly from the recording site by an amount dependent on electrotonic coupling. Computer simulations using a Purkinje fiber model confirm these theoretical and experimental results. Although off-site alternans control does not suppress alternans along the entire fiber, our results indicate that placing the node away from the stimulus site reduces alternans amplitude along the fiber, and may therefore have implications for antiarrhythmic strategies based on alternans termination.

I. INTRODUCTION

When paced rapidly, cardiac cells often exhibit a type of dynamics called repolarization alternans, which is a beat-to-beat alternation in the duration of the action potential. In the heart, such alternans induces spatial and temporal dispersion in refractoriness, which increases the risk of occurrence of potentially fatal cardiac arrhythmias. This is particularly the case when the tissue exhibits spatially discordant alternans, where different regions are alternating out of phase. Evidence of causality between alternans and the onset of reentry has been demonstrated in both experiments [1–3] and computer simulations [2,4].

Because of this link, alternans control targeted at eliminating alternans is currently under investigation as a potential antiarrhythmic strategy. Most of this work is based on model-independent, adaptive control algorithms, e.g., delayed feedback control (DFC). In this method, which is based on the Ott-Grebogi-Yorke [5] technique for chaos control, small perturbations are applied to the timing of the next excitation in an attempt to force the state of the system toward the (unstable) period-1 fixed point.

DFC has been used experimentally to control repolarization alternans in small pieces (i.e., sufficiently small to be pointlike) of bullfrog hearts [6]. DFC algorithms have also been used to control a related type of alternans [atrioventricular (AV) nodal conduction alternans; a beat-to-beat alter-

nation in the conduction time through the AV node] [7–9]. To date, AV node alternans control is the only alternans control study performed on human subjects [9].

While repolarization alternans may be successfully eliminated in an effectively zero-dimensional system that does not have wave-propagation dynamics and spatiotemporally varying repolarization, analytical work and computer simulations [10] have demonstrated that alternans control is considerably more limited in spatially extended cardiac tissue. Spatiotemporal control was investigated in a one-dimensional cardiac fiber geometry for the case where the membrane voltage is recorded at the same site as the stimulation site. For this "on-site" control scheme, the maximum fiber length in which alternans can be completely suppressed decreases rapidly with increasing distance (decreasing pacing cycle length) away from the alternans bifurcation in both theory and experiments. As a result, only very small-amplitude alternans close to the bifurcation can be suppressed in a few cm long fiber. In contrast, larger amplitude, and hence more arrhythmogenic, alternans occurring further away from the bifurcation can only be eliminated in a region of the fiber close to the stimulation site. Away from this site, alternans grow in amplitude so as to reach the maximum uncontrolled amplitude at the opposite end of the fiber. Importantly, control failure occurs even when the conduction velocity (CV) is nearly constant along the fiber and uncontrolled alternans are spatially concordant. In the more extreme case where uncontrolled alternans become spatially discordant, control is even more limited.

The inability of DFC to suppress alternans in spatially extended tissue was linked fundamentally to the wave nature

*trk2002@med.cornell.edu

of alternans in the framework of an amplitude equation that describes the spatiotemporal dynamics of alternans. This equation is derivable from the standard cable equation of action potential propagation and its parameters can be related to ionic models either analytically for simple models or numerically [11,12]. In this framework, linearly stable or unstable modes of alternans along the fiber were shown to obey a standard one-dimensional Helmholtz equation with a forcing term equal to the product of the feedback gain of the DFC algorithm and the amplitude of alternans at the recording site [11]. Interestingly, DFC completely stabilizes the spatially concordant mode, with a constant alternans amplitude along the fiber for constant CV. However, it fails to stabilize other quantized modes with a sinusoidally varying amplitude that are directly analogous to sound harmonics in a pipe. The most unstable mode among those is shaped as a half cosine wave with nearly vanishing amplitude at the pacing/recording site, reflecting successful control at this site, and maximum amplitude at the distal site, reflecting control failure. Experiments in canine Purkinje fibers [13] qualitatively confirmed this prediction.

These studies therefore suggest that spatially distributed multiple-electrode systems may be necessary in order to eliminate repolarization alternans in the heart. As a first step toward this goal, we investigate in this paper the possibility of recording action potential duration data from an "off-site," defined as a remote site with a location different than the stimulus site, and of using that information to alter pacing intervals at the stimulus site using the same DFC algorithm as in our previous "on-site" investigation [13], where the pacing and recording site coincided. This investigation is directly motivated by the wave nature of alternans. With off-site DFC, stability modes of alternans are governed by the same Helmholtz equation, albeit with a forcing term proportional to the alternans amplitude at the off-site, as opposed to the stimulation site for on-site control. As a result, the most unstable quantized mode of alternans has a node that almost coincides with the recording site. This leads to the important prediction that alternans can in principle be eliminated at a desired location that can be far away from the stimulus site.

We confirm this prediction by both experiments on canine Purkinje fibers and computer simulations of a coupled map model. The simulations also confirm the theoretical prediction that the small deviation of the node location from the recording site increases with electrotonic coupling strength, even though this deviation is practically too small on the scale of the fiber length to be resolved accurately in the present experiments.

II. METHODS

A. Ex vivo recordings

Adult dogs of either sex were anesthetized with Fatal-Plus (390 mg/ml pentobarbital sodium; Vortech Pharmaceuticals; 0.2 mg/4.5 kg iv) and their hearts removed rapidly via a left thoracotomy and placed in cold oxygenated Tyrode solution containing (in mM): MgCl, 0.7; NaH$_2$PO$_4$, 0.9; CaCl$_2$, 2.0; NaCl, 124; NaHCO$_3$, 24; KCl, 4; glucose, 5.5. Free-running unbranched cardiac Purkinje fibers (1.6–2.4 cm long, 2–3

mm wide; $n = 7$ fibers from seven animals) were excised and mounted in a tissue bath where they were superfused with warmed (37 °C) oxygenated Tyrode solution maintained at normal pH.

Pacing stimuli (rectangular pulses of 2 ms duration and $2\times$ diastolic threshold intensity) were delivered to one end of the fiber via a bipolar electrode. Action potentials were recorded (sampled at 1 kHz with 12 bit resolution [13]) simultaneously from six sites along the fiber using standard microelectrode techniques. Following 60 min of equilibration at a pacing cycle length ($T^\star$) of 300 ms, $T^\star$ was decreased progressively by 10 ms decrements to induce alternans, which were either concordant (i.e., all spatial regions alternate in phase) at slower pacing rates or discordant (i.e., distinct spatial regions alternate out of phase) at faster pacing rates. The pacing protocol subsequently was repeated with the application of the control algorithm at each $T^\star$. For all trials, the pacing stimuli were applied to one end of the fiber. The monitoring site for the control algorithm was varied across all six recording sites, either systematically or randomly. The experimental studies were approved by the Institutional Animal Care and Use Committee of the Center for Animal Resources and Education at Cornell University.

B. Coupled maps model

Because of limitations of existing ionic Purkinje fiber models in reproducing basic experimental findings such as conduction velocity, we have utilized a coupled maps model based on that of Ref. [14]. This model is based on fits to experimental action potential duration (APD) and CV restitution curves and treats electrotonic coupling with spatial derivative terms introduced in Ref. [11]. The model equations are

$$\text{APD}_{i+1} = f(\text{DI}_i) + \xi^2 \nabla^2 \text{APD}_{i+1} - w\,\nabla\,\text{APD}_{i+1}, \quad (1)$$

$$\text{DI}_{i+1}(x_i) = T + \sum_{j=0}^{i-1} \frac{\Delta x}{\theta[\text{DI}_{i+1}(x_j)]} - \sum_{j=0}^{i-1} \frac{\Delta x}{\theta[\text{DI}_i(x_j)]} - \text{APD}_{i+1}(x_i),$$

$$(2)$$

where $f(\text{DI}_i) = 31 + 160/\{1 + \exp[-(\text{DI}_i - 43)/36]\}$ is the APD restitution curve (in ms), $\theta(\text{DI}_i) = 1 + 1.4/\{1 + \exp[-(\text{DI}_i - 7)/1.4]\}$ is the CV restitution curve (in m/s), and T is the pacing cycle length. The parameter ξ determines spatial coupling. We set $\xi = 0.1$ cm so that discordant alternans occurred at a pacing rate similar to that seen in our experiments, and $w = 0.002$ cm. No-flux boundary conditions were implemented. When Eq. (1) is discretized using forward finite differences with a three-point stencil for the Laplacian, the solution is obtained by solving a linear tridiagonal matrix system. We used a fiber length of $L = 2$ cm, which is similar to the length of an individual Purkinje myocyte, and a Δx of 0.01 cm. With these parameter values, waves reach a stationary (i.e., non-traveling) state prior to the onset of control, as is the case experimentally.

C. Alternans control

As in our previous work [13], we apply a DFC algorithm, but we now separate the stimulus site and the recording site

$$T_{n+1}(0) = \begin{cases} T^{\star} & \text{for } \Delta T_{n+1} > 0 \\ T^{\star} + \Delta T_{n+1} & \text{for } \Delta T_{n+1} \leq 0, \end{cases} \qquad (3)$$

with

$$\Delta T_{n+1}(0) = \frac{\gamma}{2}[\text{APD}_{n+1}(x_r) - \text{APD}_n(x_r)], \qquad (4)$$

where γ is the feedback gain and $T^{\star}$ is the nominal pacing period. We use $x=0.0$ cm as the stimulus site, but vary the recording site (x_r), at which successive APD values are measured, along the fiber. We use $\gamma/2=0.5$, except when otherwise noted (Fig. 6).

III. RESULTS

A. Experimental results

In a previous study, we showed that when applying alternans control from a common recording/stimulating site at the proximal end of a Purkinje fiber, alternans was diminished at that location, but persisted distal to it [13]. An example of this type of control dynamics is shown in Fig. 1(b).

To test our hypothesis that off-site control would cause an APD node to be formed at the recording site, we placed six recording electrodes equidistantly along the fiber, and systematically switched the recording site (i.e., the sensory arm) between them. The stimulus site (i.e., the effector arm) was the proximal-most electrode. This setup does indeed cause APD alternans to be eliminated at the recording site, even when this site is far as 2 cm away from the stimulus site [Figs. 1(c)–1(g)].

B. Simulation results

To investigate off-site control in more detail, we used a coupled maps model based on experimentally recorded APD and CV restitution curves (see Sec. II). When applying on-site control (i.e., $x_r=0$), APD alternans is almost entirely eliminated at the proximal end, but persists distally, in agreement with our previous experimental and theoretical results [Fig. 2(b)] [13]. When applying off-site control using the locations corresponding to the remaining five microelectrodes in the experiments, the same phenomenon occurs: APD alternans is diminished at the recording site but persists away from it [Figs. 2(c)–2(g)].

When x_r is not located at either end of the cable, the diminishing of APD alternans manifests as an APD node (where APD is constant) separating out-of-phase regions [Figs. 2(c)–2(f)]. This node forms very close to x_r [insets in Figs. 2(c)–2(f)]. In the cases where x_r is located at either the proximal or the distal end, no node is formed, but the APD alternans magnitude displays a minimum at x_r [Figs. 2(b) and 2(g)].

Note that the ability to obtain control does not diminish with increasing x_r. Instead, the APD profiles are very near symmetric with respect to the recording site, such that the profiles for $x_r=2.0$ cm (1.6, 1.2) are mirror images of those for $x_r=0.0$ cm (0.4, 0.8). Such symmetry is found for a range of relatively slow pacing rates (yet fast enough to induce alternans). However, for faster pacing rates, the spatial
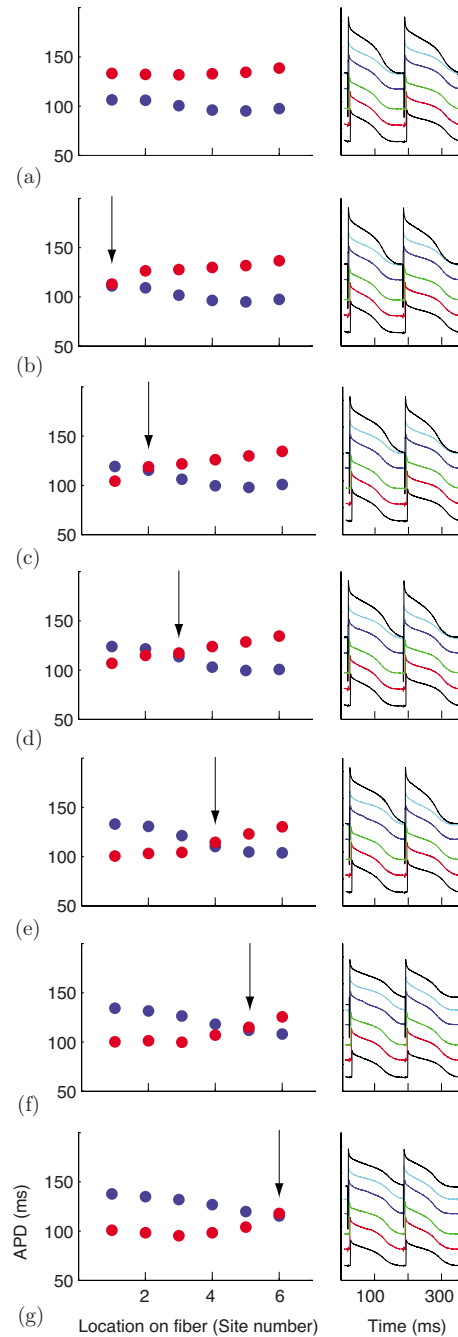

FIG. 1. (Color online) Representative example of off-site control in 2 cm Purkinje fiber stimulated from the left end. Left: APD of beat n (blue/dark gray) and beat $n+1$ (red/light gray). Right: transmembrane potential during both beats. Traces are displayed in order from top (recording site 1) to bottom (recording site 6). (a) No control and (b)–(g) control at microelectrodes 1–6 indicated by arrows. This node placement occurred robustly in seven experiments in seven different fibers.

symmetry starts to break and the APD profiles become slightly asymmetric, similar to the asymmetry observed in the experimental recordings (Fig. 1). Such asymmetry is consistent with the effects of CV restitution at fast pacing [4,15], and, indeed, in our coupled maps simulations, it disappears
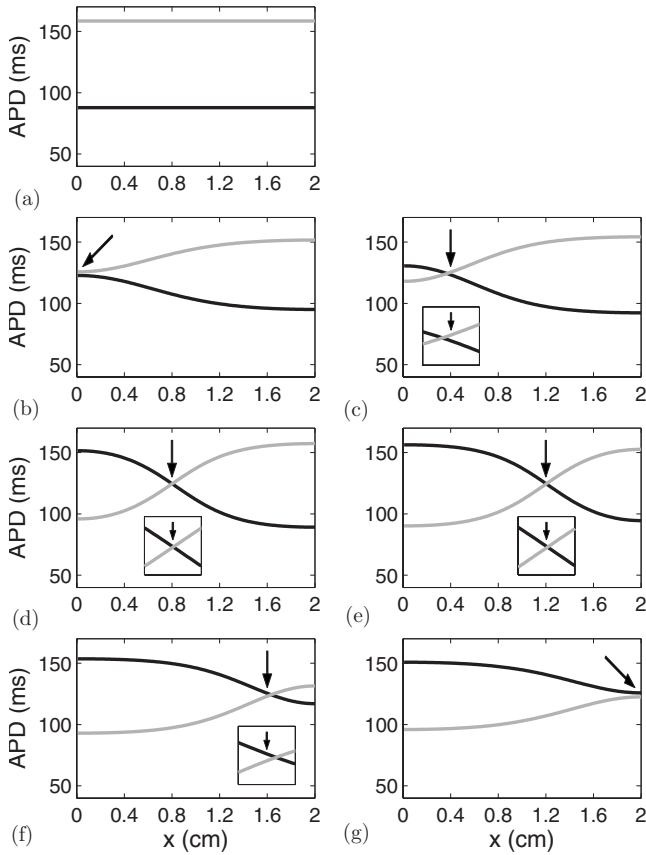
FIG. 2. Off-site control in coupled maps model with $T^\star$ $=180$ ms. Black and gray curves are obtained from two successive beats at steady state. (a) No control, (b)–(g) control at locations x_r $=0.0$, 0.4 0.8, 1.2, 1.6, and 2.0 cm (indicated by arrows). Insets show close-ups of APD node positions relative to x_r (x axes from $x_r-0.1$ cm to $x_r+0.1$ cm in each inset).

when the CV restitution function is replaced by a constant value.

At even faster pacing, a discordant node forms prior to the application of alternans control [Fig. 3(a)]. In this case, off-site control is still successful in eliminating alternans close to the recording site, but the position of the resultant node is further from x_r when x_r is near the distal end of the fiber.

Figure 4 shows a summary of the pacing-rate dependence in the simulations using the spatially averaged alternans magnitude $(\langle\Delta\text{APD}\rangle=1/L\sum_{x=0}^{L}|\text{APD}_{i+1}(x)-\text{APD}_i(x)|)$ as a measure of the effect of the off-site control application. In the case of spatially uniform and relatively small-amplitude concordant alternans ($T^\star=200$ ms), alternans is eliminated throughout the fiber, both for on-site and off-site control.

Increasing the pacing rate to $T^\star=170-200$ ms causes the pre-control alternans magnitude to increase due to APD restitution. However, further reduction in the pacing interval ($T^\star=150-160$ ms) leads to a decreased pre-control alternans magnitude as CV restitution causes the long APD to decrease with distance and the short APD to increase with distance prior to the formation of discordant alternans (at $T^\star=140$ ms). Despite these significant changes in alternans dynamics within the concordant alternans range, application of nonlocal control for $T^\star=150-190$ leads to local APD con-
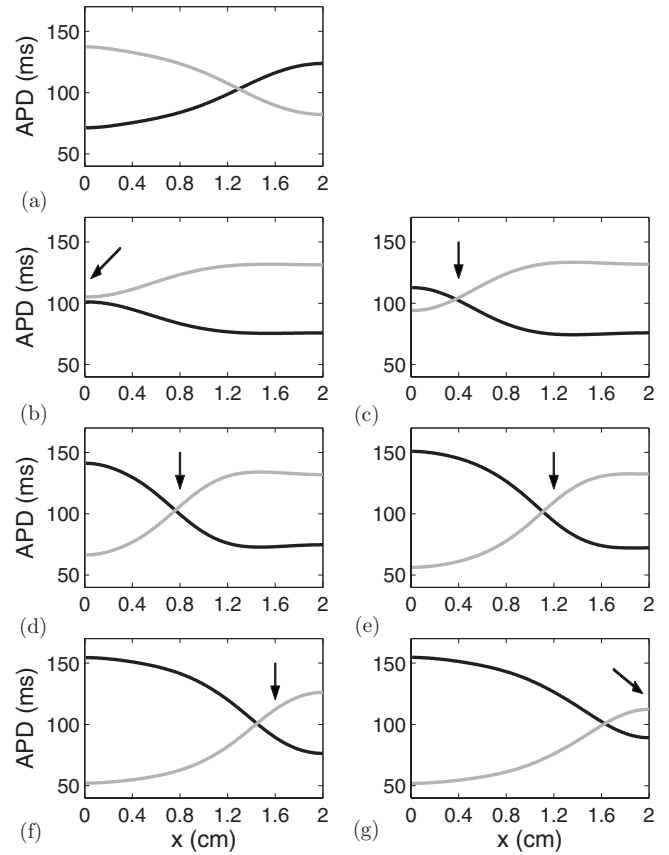

FIG. 3. Off-site control of spatially discordant alternans in coupled maps model with $T^\star=140$ ms. (a) No control and (b)–(g) control at locations $x_r=0.0$, 0.4 0.8, 1.2, 1.6, and 2.0 cm (indicated by arrows).

trol and a reduction in the alternans magnitude compared to pre-control.

This figure also demonstrates the existence of spatial symmetry with respect to x_r and its breakdown during very fast pacing. For $T^\star=170-190$ ms, letting $x_r=0.0$ (or 0.4 or 0.8) gives almost identical values of $\langle\Delta\text{APD}\rangle$ as setting $x_r=2.0$ (or 1.6 or 1.2, respectively). However, for $T^\star\leq160$ ms, the symmetry is broken for {0.4, 1.6} and {0.8, 1.2}, while for $T^\star\leq150$ ms, the {0.0, 2.0} cases also result in different values of $\langle\Delta\text{APD}\rangle$.

C. Theoretical predictions of node placement

In order to obtain a quantitative description of the physics underlying off-site control, we employed a theoretical approach building on a wave equation of the alternans amplitude [11,10]. For this analysis, we found it simpler to consider the control scheme where the pacing interval is modified at every beat, irrelevant of the sign of ΔT_{n+1}, as opposed to the control scheme in Eq. (3).

The APD at the nth beat along the cable for the fundamental standing wave mode, neglecting CV restitution effects, is given by

$$\text{APD}^n = \text{APD}_c + (-1)^n a(x), \qquad (5)$$

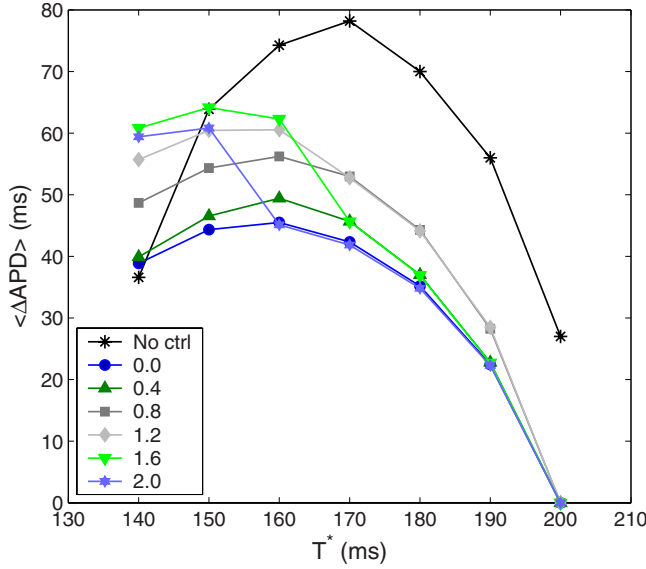where APD_c is the APD at the periodic fixed point of the map and a is the alternans amplitude given by

FIG. 4. (Color online) Effects of off-site control on average alternans amplitude ($\langle \Delta APD \rangle$). Numbers in inset indicate values of x_r. Prior to control, there is spatially concordant alternans for pacing-rates $T^\star = 150$–190 ms and spatially discordant alternans at $T^\star = 140$ ms.

$$a(x) = A_1 \left[\cos\frac{\pi x_r}{L} + \left(\frac{2\pi^2 \xi^2}{\gamma L^2} - 1 \right) \cos\frac{\pi x}{L} \right], \qquad (6)$$

where ξ is the spatial coupling length and L is the fiber length. This amplitude is the first quantized alternans mode (arising from the largest eigenvalue; see Appendix for a derivation). Figure 5 shows the resulting alternans amplitude spatial profiles for the same values of x_r as used in Figs. 1–4. For each x_r value in Fig. 5, A_1 was computed as $A_1 = \frac{a(L) - a(0)}{2(1 - 2\pi^2 \xi^2)/(\gamma L^2)}$, where the values of $a(0)$ and $a(L)$ were taken from the coupled maps simulations in order to match the alternans amplitude difference between the two ends of the cable. The resulting profiles are quite similar to those obtained from the simulations and the experiments. Further, theory, simulations, and experiments all show very close agreement in terms of node placement.

The position x_0 of the node is found by setting $a(x_0) = 0$, which gives,

$$x_0 = \frac{L}{\pi} \cos^{-1} \left[\frac{1}{1 - (2\pi^2 \xi^2)/(\gamma L^2)} \cos\frac{\pi x_r}{L} \right]. \qquad (7)$$

The curve x_0 versus x_r therefore has a point symmetry about the center of the cable. For $\xi = 0$ (negligible diffusive coupling), this curve is a line, meaning that the node and the recording site coincide. For finite coupling, however, a node only forms when $x_r^{\min} \leq x_r \leq x_r^{\max}$ where

$$x_r^{\min} = \frac{L}{\pi} \cos^{-1} \left[1 - \frac{2\pi^2 \xi^2}{\gamma L^2} \right], \qquad (8)$$
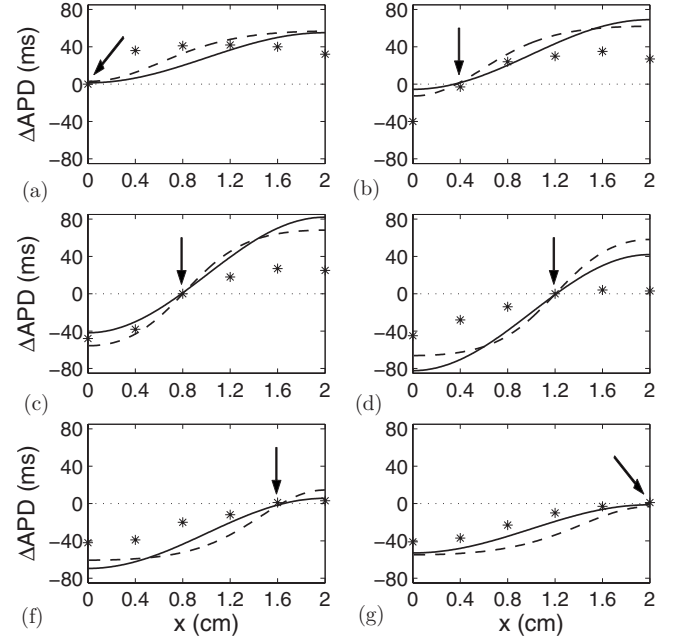
and by symmetry

FIG. 5. Alternans amplitude (ΔAPD) profiles with off-site control applied at locations $x_r = 0.0$, 0.4 0.8, 1.2, 1.6, and 2.0 cm (indicated by arrows). Theoretical profiles (solid lines) are computed from Eq. (6) with $A_1 = 28.2$, 39.2, 65.1, 65.4, 39.5, and 27.1 ms for panels (a)–(f). Also shown are results from coupled maps simulations (dashed lines) with $T^\star = 180$ cm (as in Fig. 2) and experimental data (asterisks; same preparation as in Fig. 1).

$$x_r^{\max} = L - x_r^{\min}. \qquad (9)$$

The node position varies continuously from 0 to L as x_r varies from $x_r^{\min}$ to $x_r^{\max}$. For x_r smaller than $x_r^{\min}$ or larger than $x_r^{\max}$, there is no node; the amplitude of alternans is reduced by control but does not vanish—exactly what we see in our simulations. Further, this result shows that the deviation between the recording site and the node position is dependent upon electrotonic effects.

Figure 6(a) shows plots of the node position for different values of the feedback gain parameter γ. Interestingly, decreasing the feedback gain increases $1/[1 - (2\pi^2 \xi^2)/(\gamma L^2)]$, and hence increases the departure from a straight line. The same phenomenon is observed in our simulations [Fig. 6(b)] but could not be validated in our experiments for which the spatial resolution is insufficient to pick up such small differences in node position.

IV. DISCUSSION

Previous studies have suggested that elimination of repolarization alternans in spatially distributed systems using a common measuring/stimulus site is not possible over very large distances [10,13]. Here, we use different measuring and stimulus sites to show that alternans may be controlled at designated locations far from the stimulus site. Such node placement not only robustly manifests over a large range of values of the feedback gain, but depends predictively on the gain.
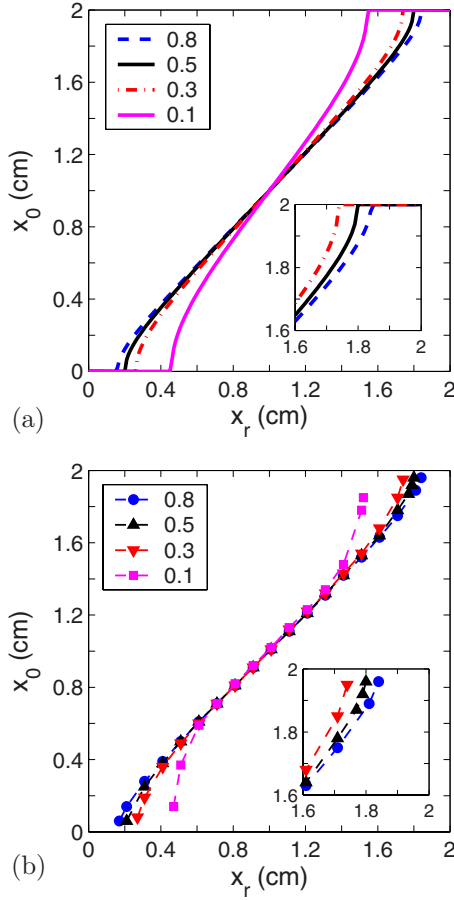
FIG. 6. (Color online) Dependence of node position (x_0) for off-site control on the feedback gain, $\gamma/2$. (a) Analytical results [Eq. (7)]. (b) Simulation results. Both sets of data are obtained for $\gamma/2=0.8$ (blue), 0.5 (black), 0.3 (red), and 0.1 (magenta).

The spatial alternans magnitude profile is well described by a theoretically described amplitude equation, which also predicts quantitatively the node placement. These findings thus further confirm the wave nature of alternans.

A. Time scale of alternans control

Upon turning on control in both simulations and experiments, the new steady state is reached after a transient lasting typically on the order of tens of beats. This occurs for most values of the feedback gain, except those that are very close to the critical value where the ability to control is lost. Indeed, unless the feedback gain is close to critical, for a short fiber (where conduction velocity restitution is insufficient to cause spatially discordant alternans without control) one first sees a relatively fast decay of the concordant mode with a spatially constant alternans amplitude, followed by a slower establishment of the spatially varying mode with a node near the control point. Since the amplitude of alternans relaxes diffusively without conduction velocity restitution in a short fiber, the relaxation time of this mode should scale as $t \sim L^2/D$, where D is the diffusion constant. Hence, the number of beats, N, required to fully relax this mode should scale as $N \sim L^2/(DT) \approx 20$ beats, for typical values of the pacing

rate ($T=0.2$ s), the diffusion coefficient ($D=1$ cm/s), and the fiber length ($L=2$ cm).

B. Implications for whole-heart antiarrhythmic alternans control

Although off-site control does not typically eliminate alternans everywhere along the fiber, it may still be potentially important for antiarrhythmic strategies. First, because it is a step toward multiple-electrode control. Second, because it reduces the repolarization gradient in some cases [e.g., Fig. 3(c)]. And finally, because APD alternans amplitude varies spatially across the ventricles (with typically larger amplitude at the base than at the apex). Hence, control may be most antiarrhythmic by modifying the pacing period as a function of the APDs measured where alternans amplitude is largest in the absence of control.

APPENDIX

Following the same notation as in Ref. [10], the amplitude equation is given by

$$\tau \frac{\partial a}{\partial t} = \sigma a - b - w \frac{\partial a}{\partial x} + \xi^2 \frac{\partial^2 a}{\partial x^2}, \tag{A1}$$

$$b(x) = b(0) + \frac{1}{\Lambda} \int_0^x dx' a(x'), \tag{A2}$$

subject to the boundary condition

$$b(0,t) = \gamma a(x_r, t)/2, \tag{A3}$$

which corresponds to the DFC algorithm of Eq. (3) with the recording site located at $x=x_r$. Note that this algorithm only permits a reduction in the pacing interval, as opposed to both a reduction and an increase in that interval as in the scheme considered in Ref. [10]. The latter unrestricted algorithm, with control applied at every beat, would yield the boundary condition $b(0,t) = \gamma a(x_r,t)$, and thus yield identical predictions up to a factor of two in the value of the feedback gain.

The stability of spatially uniform state without alternans [$a(x,t)=0$] is readily analyzed by substituting

$$a(x,t) = \exp(\Omega t/\tau) \Psi(x; \Omega), \tag{A4}$$

into the amplitude equation. We then look for solutions of the resulting eigenvalue problem that can be written in the form of a forced Helmholtz equation

$$\xi^2 \frac{d^2\Psi}{dx^2} + (\sigma - \Omega)\Psi = \frac{\gamma}{2}\Psi(x_r) + w\frac{d\Psi}{dx} + \frac{1}{\Lambda}\int_0^x dx' \Psi(x'), \tag{A5}$$

subject to the boundary conditions

$$d\Psi/dx = 0 \quad \text{at} \quad x = 0, L. \tag{A6}$$

Neglecting the last two terms on the right-hand side of Eq. (A5) for a short cable, the forcing becomes a constant, $\gamma\Psi(x_c)/2$. The eigenvalues and eigenvectors are now given by

$$\Omega_0 = \sigma - \frac{\gamma}{2} \quad \text{with} \quad \Psi_0 = A_0, \tag{A7}$$

and for $n \geq 1$

$$\Omega_n = \sigma - \frac{n^2 \pi^2 \xi^2}{L^2}, \tag{A8}$$

$$\Psi_n = A_n \left[\cos\frac{n\pi x_r}{L} + \left(\frac{2n^2 \pi^2 \xi^2}{\gamma L^2} - 1 \right) \cos\frac{n\pi x}{L} \right], \tag{A9}$$

where $\sigma = \ln f'$.

[1] J. M. Pastore, S. D. Girouard, K. R. Laurita, F. G. Akar, and D. S. Rosenbaum, Circulation **99**, 1385 (1999).

[2] J. J. Fox, M. L. Riccio, F. Hua, E. Bodenschatz, and R. F. Gilmour, Jr., Circ. Res. **90**, 289 (2002).

[3] M. Chinushi, D. Kozhevnikov, E. B. Caref, M. Restivo, and N. El-Sherif, J. Cardiovasc. Electrophysiol. **14**, 632 (2003).

[4] Z. Qu, A. Garfinkel, P.-S. Chen, and J. N. Weiss, Circulation **102**, 1664 (2000).

[5] E. Ott, C. Grebogi, and J. A. Yorke, Phys. Rev. Lett. **64**, 1196 (1990).

[6] G. M. Hall and D. J. Gauthier, Phys. Rev. Lett. **88**, 198102 (2002).

[7] K. Hall, D. J. Christini, M. Tremblay, J. J. Collins, L. Glass, and J. Billette, Phys. Rev. Lett. **78**, 4518 (1997).

[8] D. J. Christini and J. J. Collins, Phys. Rev. E **53**, R49 (1996).

[9] D. J. Christini, K. M. Stein, S. M. Markowitz, S. Mittal, D. J. Slotwiner, M. A. Scheiner, S. Iwai, and B. B. Lerman, Proc. Natl. Acad. Sci. U.S.A. **98**, 5827 (2001).

[10] B. Echebarria and A. Karma, Chaos **12**, 923 (2002).

[11] B. Echebarria and A. Karma, Phys. Rev. Lett. **88**, 208101 (2002).

[12] B. Echebarria and A. Karma, Phys. Rev. E **76**, 051911 (2007).

[13] D. J. Christini, M. L. Riccio, C. A. Culianu, J. J. Fox, A. Karma, and R. F. Gilmour, Jr., Phys. Rev. Lett. **96**, 104101 (2006).

[14] J. J. Fox, M. L. Riccio, P. Drury, A. Werthman, and R. F. Gilmour, Jr., New J. Phys. **5**, 101 (2003).

[15] M. A. Watanabe, F. H. Fenton, S. J. Evans, H. M. Hastings, and A. Karma, J. Cardiovasc. Electrophysiol. **12**, 196 (2001).